Recommended Practices in Electric Propulsion for Optical Emission Spectroscopy

Kentaro Hara*

Stanford University, Stanford, CA, 94305, USA

Vernon H. Chaplin† and Lee K. Johnson‡

Jet Propulsion Laboratory, California Institute of Technology, Pasadena, CA, 91109, USA

Gabriel Xu§

The University of Alabama in Huntsville, Huntsville, AL, 35899, USA

Deborah A. Levin¶

The University of Illinois at Urbana-Champaign, Urbana, IL, 61801, USA

1 Introduction

Characterization of the plasma and charged particle environment created in and/or by electric propulsion systems is necessary for understanding the associated fundamental physics and quantifying system performance. A wide range of techniques exist and continue to be developed to characterize different properties of plasmas of all ranges [1]. These methods can be passive and leverage the natural behavior and phenomina exhibited by the plasma to discern properties and parameters, or active where the plasma is perturbed to force a reaction that is measured to implicitly discern specific properties. Additionally, the nature of perturbation can vary from non- or semi- intrusive (such as concentrated energy injection via a laser) that limit altering the plasma

*Assistant Professor, Aeronautics and Astronautics, kenhara@stanford.edu
†Technologist, Propulsion, Thermal, and Materials Systems, vernon.h.chaplin@jpl.nasa.gov
‡Technologist, Propulsion, Thermal, and Materials Systems, lee.k.johnson@jpl.nasa.gov
§Professor, Mechanical and Aerospace Engineering Department, gabe.xu@uah.edu
¶Professor, Aerospace Engineering Department, deblevin@illinois.edu

environment to more-intrusive methods such as plasma probes. Based on the application, different techniques or combinations of techniques are employed to characterize plasma discharges to the extent that cost and complexity limitations allow. One of the most commonly used technique for plasma characterization across all disciplines, including electric propulsion, is optical emission spectroscopy (OES). The spectral emission from the plasma species, especially in the visible and near-infrared, can be measured to estimate plasma properties and composition amongst other applications [2]. Different OES techniques offer varying fidelity of information about the plasma, but in general the techniques are often used for their fundamental, passive, and non-intrusive nature. These advantages, along with the relative ease of implementation of such diagnostics, have made OES increasingly popular for electric propulsion applications. The motivation for this effort is to present the community with a set of best practices developed collaboratively by authors experienced with OES for electric propulsion to provide a process by which modeling, measurements, and analysis can be made repeatably across the electric propulsion community.

1.1 Applications of Optical Emission Spectroscopy

Optical emission spectroscopy is used in numerous fields deadling with plasma discharges as the techniques offer a simple, cost-effective, and direct characterization. As light is naturally emitted by the discharge due to species excitation, OES provides a passive mechanism to characterize the plasma without intrusively perturbing the environment or inducing any transient behaviors. Additionally, as these emissions are naturally occuring, they provide a direct and fundamental pathway to directly evaluate plasma properties. The detection and transfer of light is fundamental to many technologies and therefore numerous detectors and transfer components have been developed commercially that enable cost-effective systems that can be developed for plasma characterization. Furthermore, detection of light is much less constrained spatially and temporally than many other plasma diagnostics, allowing OES to be used in almost all spatial and temporal scales and systems.

The plasma spectrum provides invaluable insight into the composition and properties of the plasma. The wavelenths of emission identify transitions unique to atomic, ionic, and molecular constituents of the plasma. The intensity, shape, broadening, and wavelength shifts of the emission lines can be used to determine plasma properties such as temperature and density. Additionally, time-resolution allows for species-based monitoring of temporal instabilities that can be used to understand more complex plasma dynamics. When applied to electric propulsion these measurements are invaluable, as descibed briefly in this section and further detailed thoughout this paper. Spectra from discharge or plume measurements can be used to understand what elements are present and determine any contribution from facility contamination. In addition to contamination, the spectra can be used to identify erosion of thruster surfaces and provide qualitative insights on how the erosion rates change with operation parameters to inform system design and lifetime considerations. Intensity ratios of different spectral lines, coupled with collisional-radiative models (CRM), can be used to determine electron density and temperature to better understand ionization and energy transfer processes in discharges and characterize thruster performance. OES provides a high density of information about the plasma's composition, behavior, and properties without interfering with the thruster's operation, making it a powerful tool for characterizing electric propulsion systems.

1.2 Plasma Regime Considerations

Optical emission spectroscopy is frequently used for characterization of plasmas of all density and temperature regimes [2, 3], such as high density fusion plasmas, cold atmospheric plasmas, high energy-density arc-discharge plasmas, and low temperature plasmas such as those commonly created in electric propulsion discharges. The density and temperature of the plasma of interest will impact the applicability and utility of different optical emission spectroscopy techniques. The optical density describes how much emitted light is attenuated or absorbed before leaving the plasma volume, and must be considered and evaluated to appropriately use the proper OES methods for a given system. If a plasma is optically thin, the medium will not significatly attenuate the emission nor cause significant line broadening, and therefore the emission intensity will scale with density of particles. These measurements can be supplemented by collisional-radiative models (CRMs) described in later sections to determine plasma properties. However, if a plasma is optically thick, then significant light emission will be reabsorbed, attenuated, or scattered before leaving the plasma volume, meaning the emission intensity will also depend on size and other properties of the plasma. This poses strong limitations on what geometric setup assumptions, CRMs, and other quantitative analysis can be applied to the data without significant additional considerations. Additionally, plasma temperature plays a fundamental role in the line broadening, state transitions, and intensity of emissions that occur from species and much be considered in context of the proposed setup and validity of analysis and application of appropriate models to the results. A notable assumption applied throughout this paper and in electric propulsion applications is that electron energy distributions are Maxwellian, directly affecting how temperate is interpreted and models are treated.

As optical emission spectroscopy can cover a range of techniques and diagnostics, and electric propulsion represents multiple different plasma systems, the scope of this paper will be narrowed to focus on more commonly/frequently used techniques and types of propulsion systems. Namely, the scope shall be focused on OES practices for Hall-effect thrusters (HETs) operating on xenon, krypton, and argon. Much of the paper will detail best practices and examples for theory/modeling of OES for EP, different measurement techniques and their applications, and experimental considerations. Section 2 discusses in detail the best practices for theory and modeling, including details on rate coefficients for models, corona discharge models available in the literature and how they are used, and collisional-radiative models for low-temperature plasmas for xenon and argon along with references and examples for use in plasma property estimation. Section 3 details different applications that OES is used for such as contamination identification, plasma property estimation, and irradiance measurement. This section will also detail the process by which these techniques are implemented, the advantages and limitations of each, and the general requirements. Section 4 overviews considerations and engineering setup for different techniques and best practices for optics design/setup, fiber optics sizing, different sensor types, and calibration and analysis best practices to ensure proper measurements. Finally, section 5 discusses current topics in electric propulsion that do not yet have the same volume of literature in the field to recommend best practices but warrant additional discussion, such as alternative propellants, thruster systems, and data-driven models. The authors aim to provide the community with a collaborative set of guidelines for optical diagnostic implementation in the laboratory setting from academic institutions to commercial companies, as well as provide modelers and experimental scientists with input on requirements/considerations from the other to inform better experiment design or modeling input.

2 Theory and Modeling

The light emitted from a plasma discharge is created by combinations of collisions of species, excitation and de-excitation of electronic states within atoms, and vibrational and rotational behavior of molecular species. In electric propulsion, the propellants are typically atomic and theefore the emission processes are dominated by collisions and electronic state excitations. As these processes are quantized, measurements of the emitted frequencies can be back-propagated to determine the processes that occured to produce that specific emission. To derive useful information about plasma properties from these processes, a model is generally required that describes how the atomic energy level populations depend on the electron temperature (T_e), electron density (n_e), and sometimes other properties such as the neutral density (n_g) and electron and ion mean flow velocities (u_e and u_i). In this section, the mechanisms causing optical emission in electric propulsion plasmas are overviewed in more detail. Corona discharge models and collisional radiative models are then described in detail including recommendations on resources for collision rates and line ratios for xenon density and temperature measurements.

2.1 Corona Discharge Models and Local Thermodynamic Equilibrium

In very high density plasmas where the rates of electron-impact excitation and de-excitation dominate over spontaneous emission, the energy level populations tend toward a Boltzmann distribution in which each excited state k has population density $n_k \propto g_k \exp(-E_k/k_B T_e)$, where g_k is the statistical weight of state k, E_k is its energy with respect to the ground state, and k_B is the Boltzmann constant. This is called the local thermodynamic equilibrium (LTE) regime [4]—it is not relevant for Hall thrusters or gridded ion thrusters but "partial LTE", in which the populations of energy levels above some threshold level follow a Boltzmann distribution [5], may be a useful approximation for very high power density plasma sources such as magnetoplasmadynamic (MPD) thrusters. Note, however, that a laboratory plasma in which ionization is balanced by diffusive losses rather than three-body recombination may not be in partial LTE even at densities that would meet the criterion if achieved in a large-volume astrophysical plasma [6].

In the opposite, low electron density limit, called "coronal [or corona] equilibrium", electron collisions with the heavy particles are rare enough that atoms or ions that are collisionally excited have negligible probability of experiencing another electron collision before they radiatively decay back to the ground state [4]. In this case, assuming the line integrated density of the atoms/ions is low enough that radiation trapping is not significant (i.e. optically thin), the intensity of a given emission line arising from a transition between state k and state j is straightforward to calculate as a function of T_e and n_e if the excitation cross section $\sigma_{gk}(E)$ of state k from the ground state (where E is the energy of the incident electron) and the radiative transition rates A_{ki} (also called the "Einstein A coefficients") for all lower energy states i to which state k can spontaneously decay are known.

The rate coefficient for electron-impact excitation from state j to state k is calculated by averaging the product of the collision cross section and the incident electron speed v (where v_n, the neutral velocity, is much less than v_e, the electron velocity, so relative velocity $g = v_e - v_n = v_e = v$) over the electron velocity distribution function f_e:

$$K_{jk} = \langle \sigma_{jk}(v)\, v \rangle = \int \sigma_{jk}(v)\, v f_e(\boldsymbol{v}; \boldsymbol{u_e})\, d^3\boldsymbol{v}, \tag{1}$$

where the distribution function, $f_e(\boldsymbol{v};\boldsymbol{u}_e)$, depends on both the three components of electron velocity and on the mean velocity vector and K_{jk} is expressed in m^3/s in SI units. The rate coefficients are functions of the electron energy distribution function (EEDF). A kinetic description of the electrons is required to obtain non-Maxwellian EEDFs. A well-accepted approach in the low temperature plasma community is to use the local approximation. For instance, the electron Boltzmann equation with the local approximation can be used to estimate the EEDFs [7]. The rate coefficients can be used as a function of local reduced electric field (E/N) or mean electron energy. If a simpler approximation is preferred, it is also common to assume a Maxwellian distribution which is sometimes allowed to have a mean velocity in one direction:

$$f_e(\boldsymbol{v};\boldsymbol{u}_e) = \left(\frac{m_e}{2\pi k_B T_e}\right)^{3/2} \exp\left(-\frac{m_e}{2k_B T_e}\left(v_x^2 + v_y^2 + (v_z - u_z)^2\right)\right), \tag{2}$$

where m_e is the electron mass and the coordinate system has been defined to align the mean velocity along the z axis. To evaluate the integral in Eq. 1 for the distribution function in Eq. 2, it is useful to transform to cylindrical coordinates in velocity space, with $v_r = \sqrt{v_x^2 + v_y^2}$ and $dv_x dv_y = v_r dv_r dv_\theta$:

$$K_{jk} = \frac{1}{\sqrt{2\pi}}\left(\frac{m_e}{k_B T_e}\right)^{3/2} \int_{-\infty}^{\infty}\int_{0}^{\infty} \sigma_{jk}\left(\sqrt{v_r^2 + v_z^2}\right) v_r \sqrt{v_r^2 + v_z^2} \exp\left(-\frac{m_e}{2k_B T_e}\left(v_r^2 + (v_z - u_z)^2\right)\right) dv_r dv_z. \tag{3}$$

This integral can be evaluated numerically for measured or calculated cross section data. The contribution of the bulk electron flow velocity will only be non-negligible if it is quite large, as in the acceleration region of a Hall thruster where the azimuthal Hall current peaks, for instance.

The equation balancing the population and depopulation rates of excited state k in a corona model is then

$$n_g n_e K_{gk}(T_e, u_e) = n_k \sum_i A_{ki}, \tag{4}$$

where the sum can include transitions to the ground state g. Using Eq. 4, the radiated power per unit volume in an emission line produced by radiative decay from level k to level j, which is related to the line intensity that would be measured in an experiment by a geometric factor, is

$$P_{kj} = n_k A_{kj}\left(E_k - E_j\right) = n_g n_e K_{gk}(T_e, u_e)\frac{A_{kj}}{\sum_i A_{ki}}\left(E_k - E_j\right). \tag{5}$$

$\left(E_k - E_j\right)$ is equal to the energy $h\nu$ of the emitted photon, where h is Planck's constant and ν is the photon frequency.

Rather than compare the measured versus modeled intensities of individual emission lines, which requires absolute calibration of the light collection efficiency along the detection path, it is common to consider the ratio of two line intensities, which removes the dependence on the collection geometry (however, the relative sensitivity of the spectrometer and detector as a function of wavelength must still be accounted for unless the two lines are close together). Equation 5 shows that in the coronal approximation, ratios of line intensities from the same ionization stage will be

indepedent of the plasma density, depending only on fixed properties of the atom under study and on the electron velocity distribution:

$$\frac{P_{kj}}{P_{qp}} \propto \frac{K_{gk}(T_e, u_e)}{K_{gq}(T_e, u_e)}. \tag{6}$$

Corona models have been used to analyze EP-relevant plasmas [8, 9], and at typical densities in Hall thruster, gridded ion thruster, and helicon thruster plumes some line intensities may be accurately predicted by Eq. 5. However, the assumption of coronal equilibrium is typically not fully satisfied in EP plasmas due to the presence of metastable states with very long radiative decay rates ($\sim$ seconds) in commonly used noble gas propellants; these provide an important path for populating the radiating states observed in OES. Clearly, the accuracy of a corona model will also rely on the availability of accurate cross section data for excitation from the ground state, which will be discussed in Sec. 5.1.

2.2 Collisional-Radiative Models

In regimes between the LTE and corona model limits (i.e., the situation most common in electric thrusters), a collisional-radiative model (CRM) is the appropriate tool to support analysis of OES data. CRMs consider electron excitation and de-excitation processes beyond those included in the corona approximation and can therefore accurately predict emission line intensities and ratios if a sufficiently accurate and comprehensive set of cross section and transition rate data is available. For HET discharge applications, radiation trapping effects are typically neglected as th neutral density is on the order of $10^{19} m^{-3}$ and plasma density is on the order of $10^{16} - 10^{18} m^{-3}$, which makes the plasma optically thin.

2.2.1 Xenon Collisional-Radiative Models for Low-Pressure Discharges

Xenon has historically been the most widely used propellant for Hall thrusters and gridded ion thrusters, and a number of CR models have been developed to predict Xe I (neutral xenon) emission line intensities [10, 11, 12, 13, 14, 15, 16, 17]. Karabadzhak, Chiu, and Dressler published an influential model in 2006 [10] that was later extended to incorporate new measurements and calculations of electron-impact excitation cross sections out of the $5p^5\left(2P^o_{3/2}\right)6s\ ^2[3/2]^o_2$ metastable state [12]. This model, often called the "KCD model", remained the state of the art for interpreting Hall thruster plume spectra for over a decade. It relies on measurements of "emission excitation cross sections" for electron and ion impacts with xenon atoms in the ground state [18, 19], which were measured by irradiating a xenon gas sample with a monoenergetic electron or ion beam and measuring the radiated power in the emission line at wavelength λ_{kj} produced by a spontaneous decay from state k to state j. The measured line intensities were converted to an effective cross section using the formula

$$\sigma_{\lambda_{kj}} = \frac{I_{\lambda_{kj}} F_b}{I_b n_n G_b \left(E_k - E_j\right)}, \tag{7}$$

where $I_{\lambda_{kj}}$ is the measured emission line intensity in units of power, I_b is the intensity of the incident particle beam in particles/s, F_b is the beam divergence factor, n_n is the overall neutral gas density, and G_b is a geometric factor (proportional to the product of the effective solid angle

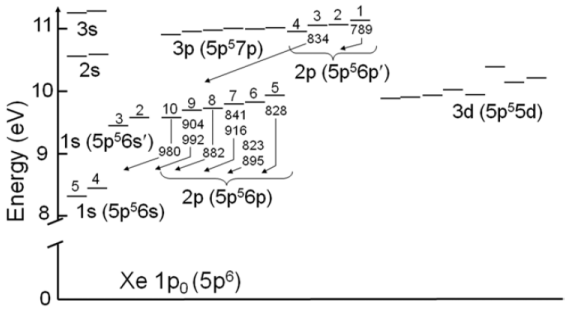

Figure 1: Xe I excited states and NIR emission lines in the KCD model. The levels are labeled using Paschen notation, with the valence electron configuration shown in parentheses. Reproduced from Ref. [12], ©IOP Publishing. Reproduced with permission. All rights reserved.

for light collection and the effective optical path length). These "cross sections" differ from the direct excitation cross section from the ground state to excited state k in that they also include contributions from excitations from the ground state to higher energy levels that radiatively cascade to level k and ultimately cause emission at wavelength λ_{kj}. This approach allows the KCD model to "incorporate the information of a significant fraction of the level-to-level radiation kinetics and the related level populations" [10] while retaining a simple model structure.

The KCD model is designed to predict the relative intensities of 11 near-infrared (NIR) Xe I emission lines originating from states with the excited electron in a $6p$ level (alternately called $2p$ states in Paschen notation). Figure 1 illustrates the energy levels and transitions in the model. The radiated power per unit volume in each emission line derived in Refs. [10] and [12] is

$$P_{\lambda_{kj}} = \left(E_k - E_j\right) n_g n_e \left(K^{\lambda}_{gk}(T_e) + \frac{n_m}{n_g} K^{\lambda}_{mk}(T_e) + \alpha K^{\lambda}_{gk,Xe^+}(E_{Xe^+}) + \frac{1-\alpha}{2} K^{\lambda}_{gk,Xe^{2+}}(E_{Xe^{2+}}) \right), \quad (8)$$

where the subscript m denotes the $J = 2$ (Paschen $1s_5$) metastable state (the other neutral metastable state with $J = 0$ is expected to have significantly lower density and is neglected in the model) and the superscript λ denotes that the rate coefficients were calculated from emission excitation cross sections. The last two terms account for ion-impact excitation, which can be important in Hall thruster plumes where T_e is low and the ions have energies of several hundred eV; α is the ratio of the singly-charged ion density to the electron density. In this model, the density n_g of xenon atoms in the ground state is assumed to be approximately equal to the overall neutral density n_n. The metastable atom density n_m is calculated from a steady-state rate equation that balances population of this state by electron-impact excitation from the ground state and radiative cascades from above with depopulation by electron-impact excitation to higher states and ionization [12].

The KCD model's predictions for the Xe I [823.2 nm] / [828.0 nm] and [834.7 nm] / [828.0 nm] line intensity ratios are shown in Fig. 2. These two line ratios have been widely used by various authors for T_e measurements in Hall thruster plumes. The [834.7 nm] / [828.0 nm] ratio calculated in the original 2006 paper [10] is shown, while the [823.2 nm] / [828.0 nm] ratio was updated in the 2009 paper [12] because the upper level of the 823.2 nm line is primarily populated by excitation from the metastable state. The close coupling of this upper level to the metastable state provides an additional source of temperature dependence for this line ratio beyond that which would be expected from the difference in $\exp\left(-E_k/k_B T_e\right)$ for the two lines: excitation of the radiating $6p$

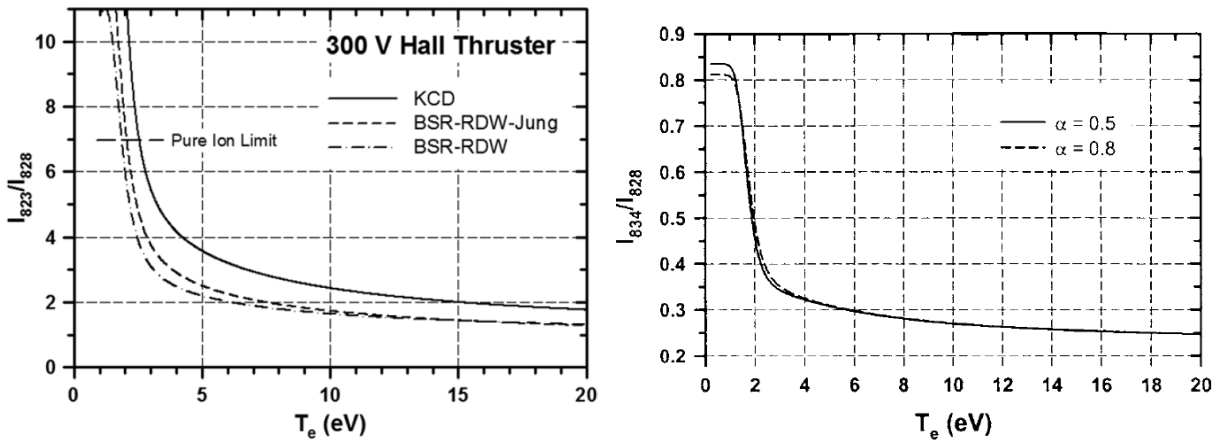

(a) (b)

Figure 2: Neutral xenon emission line intensity ratios calculated with the KCD model as a function of electron temperature. In panel (a), the middle dashed curve labeled "BSR-RDW-Jung" is likely to be the most accurate becauses it uses measured cross sections for electron-impact excitation from the $J = 2$ metastable state to the radiating $6p$ states. Reproduced from Refs. (Panel a) [12] ©IOP Publishing and (Panel b) [10] ©AIP Publishing. Reproduced with permission. All rights reserved.

state from the metastable state (Paschen $2p_6$) require an incident electron energy of only 1.51 eV, so the 823.2 nm line becomes relatively much stronger than the 828.0 nm line at low T_e even though the difference in upper level energies is only 0.11 eV.

Building an acceptably accurate Xe II (singly-ionized xenon) CR model became possible in 2019 thanks to the publication by Wang et al. [20] of a comprehensive set of electron-impact excitation cross sections and spontaneous transition rates calculated using the Dirac B-spline R-matrix (DBSR) method. This method was previously used to calculate cross sections and transition rates for neutral noble gases [21, 22] and comparisons with experimental data have shown that it predicts more accurate cross sections for incident electron energies near the excitation threshold than other available theoretical methods [12, 14]. Using these atomic data, the same group of researchers led by Zhu, Wang, and Wang published a comprehensive CR model for both Xe II and Xe I [14]. The structure of this model is similar to that of previous extensive CR models that have been published for other gases [23] in which a nearly complete set of atomic processes populating and depopulating the excited states are included in a system of rate equations to solve for the level populations, rather than lumping cascade processes together as in the KCD model. Similar models for singly-ionized and neutral xenon were published by Chaplin et al. in Ref. [16].

The CR models in Ref. [16] solve a linear system of coupled rate equations for the population of each excited state k in the model (the Xe I and Xe II models are independent, not coupled together):

$$\frac{dn_k}{dt} = \left(-\sum_{j\neq k} n_e K_{kj} - \sum_g n_e K_{kg} - n_e K_{k,iz} - \sum_{j<k} A_{kj} - \sum_g A_{kg} \right) n_k$$
$$+ \left(\sum_{j\neq k} n_e n_j K_{jk} + \sum_{j>k} n_j A_{jk} \right) + n_e \left(\sum_g n_g K_{gk} + [n_n K_{nk}] + \alpha n_n K_{nk,Xe^+} + \frac{1-\alpha}{2} n_n K_{nk,Xe^{2+}} \right). \quad (9)$$

Each term in this equation has units of density over time. As in the KCD model, depletion of the ground state density is neglected because the sum of the excited state populations is on the order of 1% of the total density in most EP plasmas; thus there is no equation for the ground state population density n_g, and terms in Eq. 9 involving transitions to and from the ground state are written separately from those between excited states for clarity. These terms related to the ground state are written as a sum over the index g because Xe II has two near-ground states with $5s^2 5p^5$ electron configurations, which are assumed to have relative populations that follow the Boltzmann equation (see Sec. 2.1).

The terms in the first set of parentheses in Eq. 9 that multiply n_k represent processes that depopulate the state k, including electron impact excitation and de-excitation to other excited states, electron-impact de-excitation to the ground state(s), electron-impact ionization, spontaneous transitions to lower excited states, and spontaneous transitions to the ground state(s). The terms in the second set of parentheses involve transitions from other excited states that populate the state k, including electron-impact excitation and de-excitation and spontaneous transitions from higher states. The terms in the final set of parentheses comprise processes that populate the state k but do not depend on densities of other excited states, including electron-impact excitation from the ground state(s), electron-impact ionization-excitation (in which a single high-energy impact ionizes a neutral atom and also excites another bound electron in the ion—this process only applies in the Xe II model), and ion-impact excitation by singly-charged and doubly-charged ions. Unlike in Eq. 8, the electron temperature dependence of the rate coefficients (as derived in Eq. 1) in not explicitly shown here for conciseness.

For a given set of input variables T_e, n_e, n_n, α, u_e (electron mean flow velocity), and E_{ion} (singly-charged ion kinetic energy), Eq. 9 may be written as a matrix equation:

$$\frac{d\boldsymbol{n}}{dt} = \mathbf{A}\boldsymbol{n} - \boldsymbol{b}, \quad (10)$$

where $\boldsymbol{n}$ is the vector of excited state populations, $\boldsymbol{b}$ is a vector composed of the constant terms in the final set of parentheses, the terms in the second set of parentheses populate the off-diagonal elements of the matrix $\mathbf{A}$, and the terms in the first set of parentheses make up the diagonal elements of $\mathbf{A}$. For a steady state solution, the left-hand side is set equal to 0, and the system may be inverted directly. Given a prescribed time dependence of the plasma parameters, time-dependent level populations may be derived by starting from an equilibrium solution, discretizing the time derivative (e.g., with a simple forward Euler method) and stepping the equation forward using time steps that are small compared to the characteristic time scales for the terms to evolve.

The model in Ref. [14] utilizes a system of rate equations similar to Eq. 9, with some additional processes included such as charge exchange, re-absorption of emitted photons within the plasma, and de-excitation of metastable atoms induced by wall collisions. The models discussed in this section were all designed for Hall thruster studies, but CR models built for most low-pressure

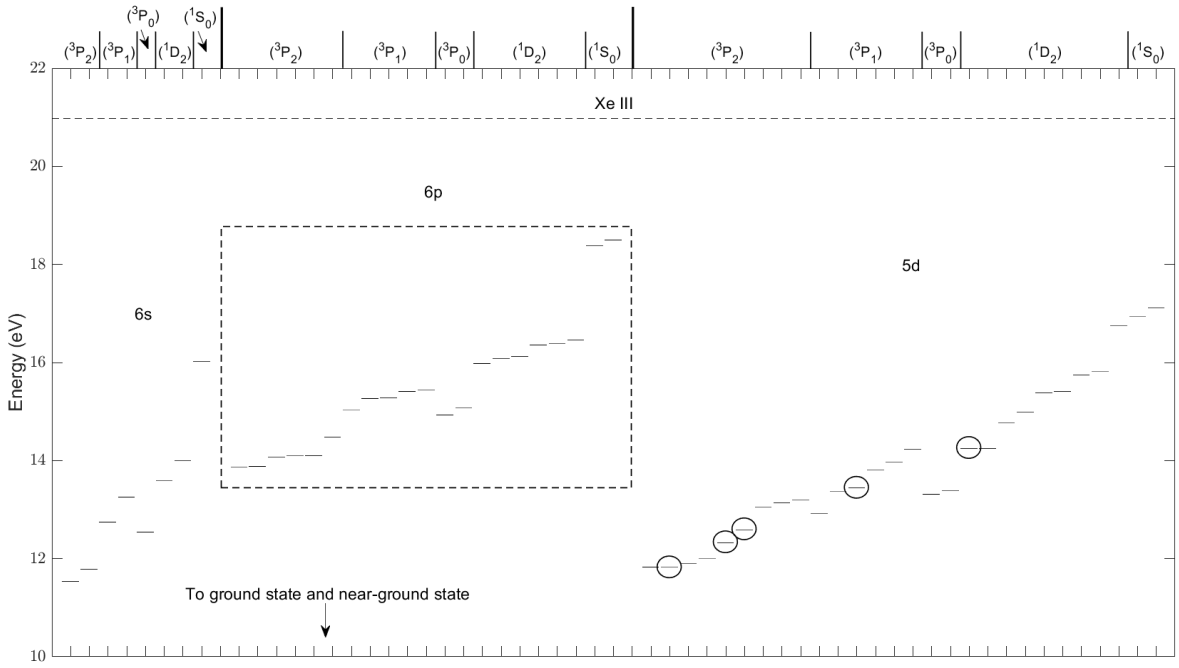

Figure 3: Diagram of Xe II energy levels included in the CR model from Ref. [16] reproduced by permission of the American Institute of Aeronautics and Astronautics, Inc. Levels are grouped according to their core angular momentum configuration. Metastable states are circled, and a dashed box surrounds the 6p states that produce the emission lines most likely be useful for OES.

partially-ionized laboratory plasma applications will generally have a similar structure, with flexibility to include other terms appropriate for specific scenarios. Key differentiators between models will be the choice of atomic data inputs (i.e., the cross sections and transition rates, discussed in Sec. 5.1) and the number of energy levels included.

The Xe I models in Refs. [14] and [16] included all excited states of xenon with an electron in the 6s, 6p, 5d orbitals, along with some higher levels (7s, 7p, and 6d). The Xe II models included all 6s, 6p, and 5d states, with no higher levels included because cross sections for populating these levels were not available. The emission lines most useful for an OES diagnostic spanning the visible and NIR portions of the spectrum all originate from spontaneous transitions between 6p and 6s states, but the 6p states are populated and de-populated through multiple pathways from other level groups, so inclusion of the additional states improves the accuracy of the results. Very high levels near the ionization energy do not need to be included because they are very easily ionized and have only moderate decay rates into the radiating states of interest, so their contribution to the observed line intensities is small. Figure 3 shows a diagram of the energy levels included in the Xe II model from Ref. [16].

While the KCD model uses a cleverly simplified structure that is well tailored to Hall thruster plume studies and can produce accurate results in the region where its approximations are valid, models that directly account for a broader set of atomic transitions allow for more detailed probing into the underlying processes producing the observed line emission, which can lead to valuable insights. For example, Fig. 4 shows an accounting of the relative importance in steady state of various populating and de-populating processes for the upper levels of the Xe I 823.2 nm and

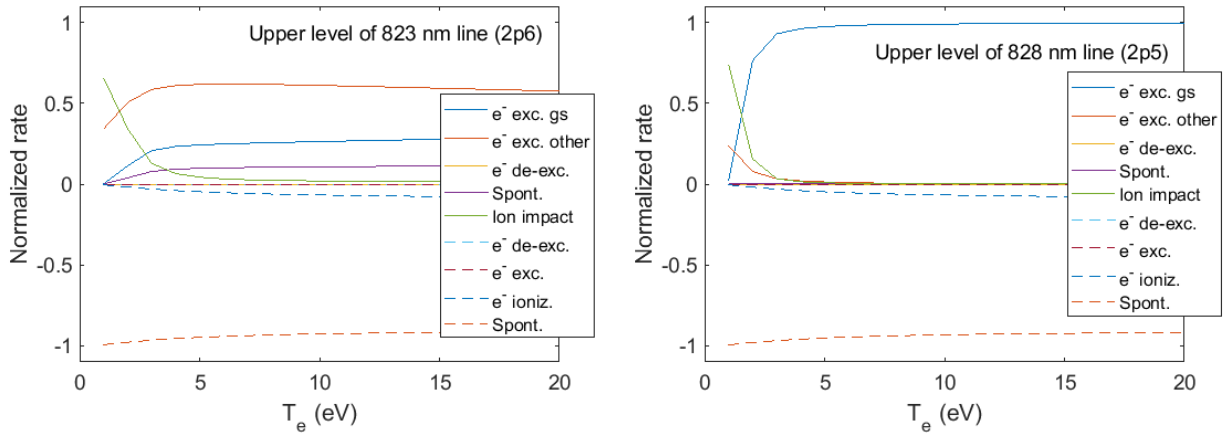

(a) (b)

Figure 4: Rates of processes populating (solid lines) and depopulating (dashed lines) the upper levels of the Xe I 823.2 nm and 828.0 nm lines calculated by the CR model from Ref. [16] assuming $n_e = 10^{18}\mathrm{m}^{-3}$. Reproduced from Ref. [16] by permission of the American Institute of Aeronautics and Astronautics, Inc.

828.0 nm lines, as a function of T_e. The 828.0 nm line's upper level is primarily populated by electron-impact excitation from the ground state, while the 823.2 nm line's upper level is primarily populated by electron-impact excitation from a metastable state, as mentioned above (this process is represented by the red curve titled "e^- exc. other" in the figure legend, which includes electron-impact excitations from all states other than the ground state). Reference [14] presents similar breakdowns of populating and de-populating processes for a number of other Xe I and Xe II levels.

Coupling of certain emission line intensities to the metastable levels has implications beyond the steady state temperature dependence of line ratios. These lines are generally ill-suited to high-speed measurements because the metastable state populations respond slowly to changes in the plasma parameters. For example, when using the line ratio's temperature dependence calculated by a steady-state CR model to derive time-dependent temperatures from high-speed OES measurements, the Xe I [834.7 nm] / [828.0 nm] line ratio will produce accurate results at oscillation frequencies exceeding 100 kHz because neither line is closely coupled to the metastable state populations, while analysis of the [823.2 nm] / [828.0 nm] ratio will produce erroneous results due to the slow response of the 823.2 nm line. The maximum oscillation frequency that a metastable-dependent line ratio can resolve is proportional to the electron density [16].

Transport of metastables can invalidate a 0-D model in some cases, particularly for ions, which can be accelerated in thruster plasmas to much greater velocities than neutrals [16]. Including 1-D or 2-D transport effects in a CR model will tend to make it prohibitively complex to directly invert the model results to derive plasma parameters through comparisons with OES data, but practically useful approaches may exist in some cases [14].

The rates of electron-impact processes populating and de-populating the metastable states are all proportional to n_e, as are the rates of electron-impact excitation from the ground state to the $6p$ states, so the KCD model predicts that the Xe I line intensity ratios depend only on T_e and are independent of the plasma density (refer to Eq. 8). However, the more complete models constructed

from Eq. 9 or a similar set of atomic processes reveal that density dependence does in fact exist for $n_e \gtrsim 10^{16}$ m^{-3}. Reference [16] uses a simplified 4-level model to illustrate that the crucial feature of the more complex CR models that causes them to predict density dependence in the Xe I line ratios is that these models allow non-metastable excited states to be depopulated by electron impacts, while these states can only be depopulated radiatively in the KCD model.

2.2.2 Xenon Collisional-Radiative Models for High-Pressure Discharges

$$\begin{aligned}\frac{dn_{2p4}}{dt} &= n_e n_g k_{g-2p4} + n_e\left(n_{1s3}k_{1s3-2p4} + n_{1s5}k_{1s5-2p4} + n_{2p}k_{2p-2p4} + n_{Ar_2^+}k_{Ar_2^+-2p2}\right) \\ &+ n_g\left(n_{1s}k_{1s-2p4} + n_{2p}k_{2p-2p4}\right) - n_{2p4}\left[A_{2p4-1s3} + A_{2p4-1s2} + n_{1s}k_{1s,2p-Ar^+} + wall\ losses\right] \\ &- n_{2p4}\left[n_g\left(k_{2p4-1s} + k_{2p4-2p}\right) + n_e\left(k_{2p4-1s3} + k_{2p4-1s5} + k_{2p4-2p} + k_{2p4-Ar_2^+}\right)\right]. \quad (11)\end{aligned}$$

At high pressures/density, typically above 1 Torr, additional neutral collisions must be incorporated into the CRM as they begin dominating the rates. For example, equation 11 is a rate equation using Paschen notation for argon 2p4 state used for an atmospheric pressure discharge. The terms on the RHS are arranged into the excitation or population of the 2p4 state (first square bracket), and deexcitation or depopulation of the 2p4 state (second square bracket). The excitation terms are in order from left the right as follows:

1. Electron collision with ground neutral argon into the 2p4 state
2. Electron collision with 1s3 neutral argon into 2p4 state
3. Electron collision with 1s5 neutral argon into 2p4 state
4. Electron collision with other 2p neutral argon into 2p4 state
5. Electron collision with ionized argon into 2p4 state
6. Ground neutral argon collision with 1s neutral argon into 2p4 state
7. Ground neutral argon collision with 2p neutral argon into 2p4 state

The deexcitation terms are:

1. 2p4 argon radiative deexcitation into 1s3 state
2. 2p4 argon radiative deexcitation into 1s2 state
3. Electron deexcitation collision with 2p4 argon into 1s3 state
4. Electron deexcitation collision with 2p4 argon into 1s5 state
5. Electron deexcitation collision with 2p4 argon into other 2p states
6. Electron deexcitation collision with 2p4 argon into doubly ionized argon
7. Ground neutral deexcitation collision with 2p4 argon into any 1s state

8. Ground neutral deexcitation collision with 2p4 argon into other 2p states
9. 1s argon deexcitation collision with 2p4 argon to produce singly ionized argon
10. 2p4 deexcitation collisions with surfaces

Equation 11 describes main rates with neutral species. This would be used if you have a weakly ionized plasma with a large fraction of neutral argon. When including neutral collisions, non-linear terms can appear which make the system very stiff and the computational solution difficult. In the equation above, the $n_{2p4}n_{1s}k_{1s,2p-Ar^+}$ term is the main non-linear one as it uses the density of two excited states, which are not known ahead of time.

3 Measurement Techniques

As introduced in sections 1 and 2, measurements of specific line emission from electric propulsion plasma discharges can provide quantitative estimates of plasma parameters and relative species concentrations. In practice there are multiple approaches to aquiring these measurements, with each technique having intrinsic and application-specific advantages and disadvantages. The properties of interest for electric propulsion spectroscopic measurements and associated techniques and resolution/capabilities are described below in Table 3. The methods can be generally classified into four catagories: (1) spectra, (2) intensity/irradiance, (3) spatially-resolved/imaging, and (4) temporally-resolved. In this section, each of the four catagories are discussed in detail included how they are typically utilized in electric propulsion and advantages and disadvantages of the techniques.

Property	Methods/Techniques	Resolution
Plasma density and temperature	Spectroscopy Spectral imaging	Spectral - multi-line ratios Spatial and/or temporal
Species identification	Spectroscopy Spectral imaging	Spectral - multi-line Spatial and/or temporal
Intensity/irradiance	Imaging Photodiode/PMT/APD	Spatial Temporal

3.1 Measurements of Spectra

Arguably the most important measurement obtained via optical emission spectroscopy is the spectrum itself of the plasma. The optical emission of electric propulsion plasmas is often dominated by line emission in the ultraviolet through the near infrared wavelength ranges (as opposed to broad emission that may be captured in the infra-red due to thermal emission processes), resulting in a spectrum that is typically ”spikey” and defined by numerous Dirac-Delta functions (narrow peaks or ”lines”) of high intensity above a low background threshold. As detailed in Section 2, the line emission is a result of specific collisions and energy transitions - therefore a plasma environment will produce a unique spectrum descriptive of the constituents it’s composed of, the relative concentration of the constituents, the energy of the particles, and the mechanisms by which different constituents interact. Specific lines in the spectrum can be attributed to different species

in the plasma, such as xenon ions vs neutrals or the presence of contaminants from thruster or facility surfaces like carbon. The ratio of xenon lines described by CRMs such as that in Section 2 can be calculated from calibrated spectrum measurements to determine electron density and/or temperature. Additionally, the intensity of propellant ion lines or carbon lines can be compared between spectra at different operating setpoints or locations to determine how ionization rates or contamination presence changes qualitatively. Finally, due to the various broadening mechanisms associated with the plasma environment (doppler, Stark, Van der Waals, or quantum uncertainty in energy levels) and instrument (finite slit width and detector size), the shape of an individual line emission will be measured as a Voight profile in shape (convolution of Gaussian and Lorentz distributions arising from the broadening mechanisms) [24]. Accurate profile measurements can enable deconvolving these distributions to determine properties such as temperature and density, though in practice this is difficult to do in electric propulsion applications due to the extremely small contribution in the LTP environment and the limited wavelength resolution of most spectrometers. The limitations of what can be accomplished from measurements of spectra are mainly dictated by the wavelength resolution of the spectrometer itself, care in system setup and calibration, and any phyical constraints of light collection.

The design of a spectroscopy system is relatively straighforward, with the most important and crucial component being the spectrometer or monochromator. Spectrometers and monochromators are composed of three fundamental elements: first an inlet optics that take in and collimate light into a beam, second a blazed grating that spectrally disperses the light beam, and third a photosensitive sensor that detects the dispersed light. Monochromators are typically narrow-band, focing on specific wavelengths in detail using slits downstream of the grating whereas spectrometers are wide range in wavelength (however some spectrometers use a monochromator with the grating on a rotation stage to produce high resolution over a wider range). The quality and specifications of each of these components results in numerous combinations of systems with different performance (wavelength resolution and range), size (compact, portable units to heavy meter long systems), and price (from 100s of dollars to 100s of thousands of dollars). Higher end spectrometers use achromatic optics for collimation to minimize the focal length distortion between different wavelengths of light that might affect measurement resolution. The density of the grating will determine how well the light is spectrally separated and ultimately resolved. The density of the gratings are commonly measured in grooves per millimeter (g/mm), with higher densities separating wavelengths finer but at the cost of overall range of wavelengths resolved. Additionally, the focal length of a spectrometer or monochromator enables higher wavelength resolution at a cost of size and portability. A photomultiplier tube (PMT) is often used as detector on monochromators with an exit slit, where the light hitting the sensor is recorded as a function of time and converted to intensity vs wavelength based on the grating position. In this instance the detector measures one wavelength at a time and the resolution is fixed by the detector area, exit slit width, and grating step size, enabling high signal sensitivity and wavelength resolution. Spectrometers typically use charge coupled devices (CCD) or complementary metal-oxide semiconductor (CMOS) cameras as detectors, where the diffracted light is projected onto the sensor face spatially and converted to wavelength based on pixel location. This results in multiple wavelength bands measured simultaneously, with the pixel size limiting the wavelength resolution but providing fast acquisition times and better relative intensities of measurements. In both cases, the measurement of spectral wavelength is derived from another property (time and/or pixel), creating uncertainty and resolution contraints as well as need for wavelength calibrations detailed in Section 4. Though not typically a factor, CCDs are

preferred over CMOS cameras as detectors due to better sensitivity in the NIR.

Another factor in selecting the proper spectrometer is the size of the system, which is defined by focal length: the distance from the focusing mirror of the spectrometer to the exit where the sensor is. A longer focal length will enable better wavelength resolution, but trade out in size, weight, portability, and cost. In typical electric propulsion applications, a compact portable spectrometer such as those available from Ocean Insight are sufficient for optical emission spectroscopy for species identification and basic line ratio estimation. A higher resolution spectrometer, such as a 1 m benchtop spectometer, will enable higher sensitivity measurements in the far plume if exploring trace amounts of facility contaminants or if attempting to finely resolve the broaded profile shape of xenon line emission for doppler broadening velocity estimation. The other components of a spectroscopy system in EP applications function to collect the light from the region of interest and transfer it to the spectrometer. This is usually accomplished using fiber optics that enable efficient transfer of light over long distances without significant attenuation or complexity. The selection of fibers for a specific application and the collection optics are detailed further in Section 4.

As earlier stated, the relative intensity of the lines (in units of counts, volts, current, or other arbitrary sensor units) can provide insight into changes in concentration and be used as ratios to estimate density and temperature. If using the line ratio approach, the system does not need to be absolutly calibrated for intensity, but does need to be calibrated for response across wavelengths of interest to account chromatic sensitivity. An additional best practice if selecting a system for line ratio implementation is ensuring all lines of interest can be resolved simultaneously, and so spectrometers are typically prefereable for this technique.

3.2 Spectral Imaging and Filterscopes

In lieu of capturing and analyzing a full emission spectrum spanning a large wavelength range, information about the plasma discharge can be captured by instead focusing on a few specific emission lines with spatial and/or temporal resolution. Spectral imaging is a powerful, high information-density technique as spatial and/or temporal characterization can be accomplished in a short timescale with a non-intrusive system that can exist outside the vacuum chamber and operate without any moving parts or motion stages for collection. For example, spatially-resolved xenon line emission images of Hall thruster discharges have been captured to understand thruster performance and near-field plume dynamics [25], or breathing mode oscillations in the discharge to understand the interplay between ion and neutral species [26, 27]. Spectral imaging can also be used to map impurity transport in the plasma from thruster channel erosion or facility contaminants, similar to how it's utilized in other fields such as fusion energy [28]. Additionally, these measurements can be made on any species to qualitatively examine spatial distributions and temporal fluctuations, such as novel propellants and non-typical propulsion systems that have been gaining interest in electric propulsion and are in need of diagnostic capabilities applicable to their characterization.

The design of spectral imaging systems can be generally grouped into one of two types. The first is the simplest design and consists of a narrow bandpass filter (centered on the wavelength of interest) or multiple bandpass filters on a filter wheel placed in front of the detector, such as that used in [25] to characterize HET plumes. The light can be piped in via fiber optic if temporal resolution is of interest, or using imaging lenses looking directly at the region of interest. The

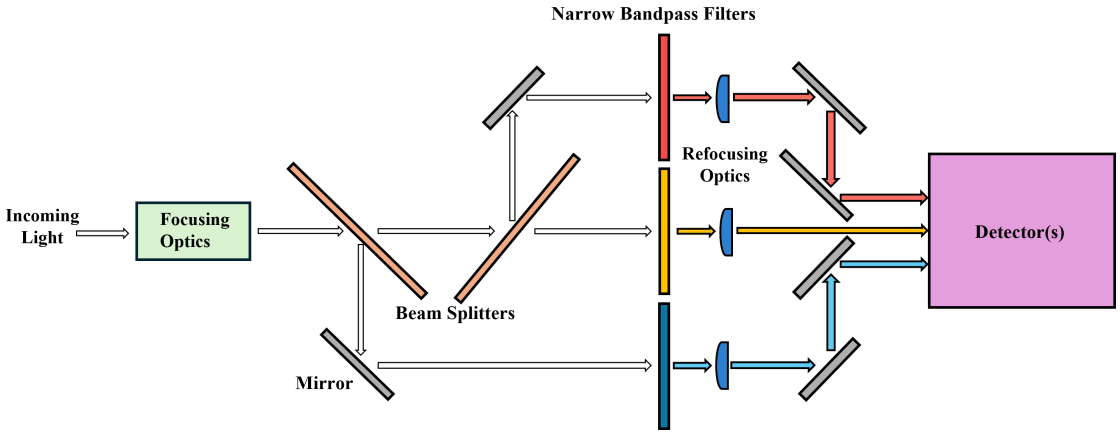

Figure 5: Generalized example of a spectral imaging system design with key components for spatially- or temporally-resolved optical emission spectroscopy.

narrow bandpass filter will block all light except that the specific emission line of interest, which is measuring using a PMT, avalanche photo diode (APD), CCD, or CMOS based on the desire for spatial and/or temporal resolution. In practice, this can be as simple as commercial bandpass filters in front of a calibrated DSLR camera and lens, and can be used to general spectral images of lines of interest. Using a filter wheel allows for measurements of multiple lines to apply line ratios or monitor multiple different species. The challenge with this approach is the triggering and/or alignment of the filter wheel and the sensor, the inability to simultaneously capture mutliple lines of interest (making this approach difficult to apply for time-varying plasmas), as well as limits on light sensitivity based on the sensor. However, this approach has may advantages including its relative simplicity, cost, and portability.

The second type of system, shown in Figure 5, is higher fidelity and used in applications requiring more spatial or temporal resolution and repeatability, such as [26, 27, 28]. In these systems, the incoming light or image is passed through beamsplitters to produce multiple light paths that can each simultaneously be individually filtered and routed to the same CMOS/camera or multiple PMTs acquiring simultaneously. This type of approach allows for simultaneous acquisition of multiple spectral lines with temporal and/or spatial resolution at the cost of some increased complexity and cost. The design can be expanded to fit as many beam paths as the user desires, though with each addition the spatial resolution will decrease as more images will need to be placed within the same sensor area, alignment complexity and errors will increase, and available signal intensity will drop due to the presence of more beam splitters. Achromatic lenses are recommended for the focusing optics to limit the bluring of the images relative to each other and introducing spatial error. Furthermore, beamsplitters are not uniformly efficient across all wavelengths meaning that additional thought needs to be given to the emission lines of interest and the location of their respective narrow bandpass filters in the system. If the application emphasis is time resolution, PMTs or APDs can be used as detectors as futher discussed in the next subsection. This reduces system complexity as the focusing optics do not need to maintain image focus, and downstream of the bandpass filters each beam can be immediately routed to the PMT rather than refocused to an imaging sensor. If spatial resolution is the primary interest, a full spectrum DSLR can be used as a detector. This will provide the greatest resolution as the pixel density is highest in these sensors and the camera's exposure and gain can be varied to obtain enough light for a clear image. A com-

promise between the two apporaches is using an intensified CCD (ICCD) or high speed camera as the sensor. Using this approach, the time resolution can be dramatically improved at the cost of decreased spatial resolution due to the reduced pixel density. Another challenge to consider is that the sensor size is often smaller and therefore alignment may be more tedious and complex. Additionally, if the measurement suffers from insufficient light reaching the sensor, a phosphor multi-channel plate (MCP) can be used to intensify the signals. However, this will limit time resolution to 10s of kHz due to the decay time of the phospher excitation. If using any of these systems, one must ensure the system is calibrated for sensor uniformity and chromatic sensitivity as detailed in Section 4. Finally, these systems can be designed with numerous commercially-available components allowing for easy exchanging of beam splitters and line filters without significantly altering alignment (though the system may need to be recalibrated), making them ideal for characterization of different plasma species or contaminants.

3.3 Time-Resolution

Most EP thrusters in use today are steady state devices, such as ion engines, Hall effect thrusters, electrosprays, field-emission electric propulsion (FEEP) systems, resistojets, and arcjets. Pulsed or quasi-steady thrusters are also a strong area of research, including micro cathode arc thrusters (μCAT), pulsed magnetoplasmadynamic (MPD) thrusters, pulsed plasma thrusters (PPTs), or radio-frequency (RF) thrusters. If one is interested in the non-average plasma behavior for these pulsed systems or oscillations in the steady state devices, then temporal resolution of the measurement is important to consider as mentioned in the previous section. Additionally, in the broader area of plasma physics, there are many plasma phenomenon that are short duration in nature either due to the energy requires to generate them (fusion, magnetic reconnection), or due to a desire to reduce total energy deposition (dielectric barrier discharges or atmospheric plasmas). These time-varying plasmas still produce the same emission spectra as steady state plasmas, but to fully characterize the plasma behavior requires capturing emission spectra at short-time scales.

The necessary minimum time-scales depend heavily on the experiment and the controlling phenomenon. For example, if you want to study the time-resolved plasma in a 13.56 MHz RF plasma, then the maximum time-scale would be based on one RF cycle, or 74 ns. For a μCAT, the maximum time-scale is based on the discharge time which is on the order of 1 μs to 10 μs. The minimum time-scale is set by the diagnostic equipment, when the plasma is expected to change, or the speed at which atomic energy level populations can respond to changes in the plasma (limited by the electron-impact excitation frequency and the spontaneous decay rate of relevant levels). Specific equipment will be discussed in more detail later, but in general there are three passive detector options, high speed photodetectors or PMTs, fast-gate ICCD cameras, or high frame rate CMOS cameras. They each have their benefits and limitations. Photodetectors are single channel detectors, thus they provide no spatial information, but can obtain bandwidths in the 10s of GHz with standard commercial units. This means the temporal resolution, or the time step of each data point is 0.1 ns.

ICCD cameras can capture a “picture”, thus they have spatial resolution. They have fast gates or fast shutters down to the 100’s ps, though more commonly the 1 ns range. However, they typically have very low frame rates around 10 fps. These factors mean they can capture a full picture of the plasma at a given instant, but only one image per plasma cycle or discharge. The ps-ns gate speed essentially allow you to “freeze” the plasma in time and only capture the photon emissions from

the period of time and study it. However, the emission from 1 ns time period is often very small, unless it is an exceptionally energetic plasma. Thus, a single capture from a single plasma cycle or discharge is often insufficient to obtain high signal-to-noise for useful data. To overcome this, ICCD cameras have an intensifier, the I part, which amplifies the raw emission by 100's of times. The drawback is the amplification is non-selective and will amplify both the desired signal and the undesired noise. To overcome this limitation, ICCD cameras often add multiple captures together, something called multiple accumulations. This can be done manually in post-processing, though most ICCD camera software has the option built in. By summing multiple accumulations, both the signal and noise are increased, but hopefully the signal is larger than the background noise and the summing allows the signal to show through. If the noise is primarily due to random sources such as dark currents on the CCD or background radiation, then averaging the captures can reduce the noise while maintaining the signal level. A common technique is to accumulate multiple captures in summing mode to obtain higher signal, save that data set, then repeat for 5 total data sets which are then averaged to reduce the noise floor. This technique requires the plasma be highly repeatable as each accumulation is a different cycle or discharge. It also requires the camera to be synchronized to the discharge. This is typically done using some characteristic trigger. The trigger can either be external from a signal generator that controls both the plasma and the camera, or can be captured from some plasma signal (current or voltage sensor, photodetector, probe, etc.).

High-speed cameras typically use CMOS sensors and can have millions of frame rates per second, though often times with a reduced sensor area. However, they have slower gate or shutter speeds, which typically scales with the frame rate. For example, a 1 Mfps maximum framerate would have a minimum gate time of 1 µs. If operating at lower frame rates, the gate time can typically be increased by the user. Thus, high-speed cameras can capture multiple images from a single plasma cycle or discharge, but with less temporal resolution for each image. Summing and averaging can also be done with these cameras, but are not common as the larger gate times usually allow sufficient light to be captured.

In recent years, the ability to couple an intensifier to a high-speed CMOS camera has become commercially available. These are either sold as an intensified relay optic (IRO) device that attaches to the CMOS camera like a lens, or may be fully integrated to produce an intensified CMOS system. This combination potentially allows you to obtain both high-speed Mfps frame rates and nanosecond scale gate times. One limitation of these coupled devices is the loss of some spectral information. This is due to the way CMOS and CCD sensor differ. CCD sensors can detect photons from the UV to low IR (200-900 nm), while CMOS sensors only detect photons in the visible spectrum (400-700 nm). Thus, a CMOS camera cannot see the UV emissions from the plasma, for example argon ion lines. The IRO however can see the UV photons, and can amplify the raw signal just like in the CCD. But, to turn that signal into something the CMOS sensor can detect, the IRO converts all the light into a visible wavelength, typically around green. One limitation of direct imaging is the loss of spectral details. While CCD sensor can detect UV-IR photons, the sensor itself only reads out the current in each sensor pixel, thus providing only an intensity measurement. Thus, these cameras are often coupled to spectrographs to form a spectrometer as previously described in order to obtain wavelength data.

The last consideration for time-resolved spectroscopy is finding the necessary time delay to capture the phenomenon of interest. Cameras have an insertion delay, which is the minimum time between when the trigger signal reaches the camera to when the camera opens its shutter and can take data. This is typically on the order of 10's of ns, but is an unavoidable delay. In addition, there

may be delays due to line lengths or other equipment in the system. Electronic signals travel at about the speed of light in wires, thus there is a signal delay of 3.3 ns/meter of cable that is carrying the trigger to the camera. For most experiments, a minimum delay of 100 ns is acceptable as the plasma itself may not begin forming until after that time. However, some experiments, in particular laser based ones, require more attention. If the phenomenon or time of interest will occur within the minimum insertion delay time, then there are two options to enable measurement. The first is to use an external trigger source to initiate both the plasma and camera, and send the camera trigger signal slightly before the plasma trigger such that the camera shutter will open when desired. The second option is to use what is called "the second shot" if the plasma is highly repeatable. For example, a pulsed laser will typically fire and hit the target before the camera can open its shutter. Thus, if the camera is triggered from the laser electronics, it may miss the laser hitting the target. The second shot solution is to fire two laser pulses with a known separation time, say 1 second. Then over delay the camera trigger such that the first pulse triggers the camera, but the shutter doesn't open until when the second pulse would fire.

4 Experimental Considerations

While optical emission spectroscopy is a generally simple diagnostic from experimental and implementation considerations, special care must be taken with certain aspects to ensure fidelity of the measurements and minimize errors. These include more minute details such as appropriate selection of optics and full calibration of the spectroscopy system before and/or after each experiment or test campaign. The previous section presented experimental techniques from a larger perspective of what measurements can be attained and the types of systems, with associated benefits and constraints, to enable those measurements. In this section, the details of experimental considerations are discussed in context of typical electric propulsion applications, beginning from the optics setup, to system calibrations, then noise sources and improving measurement signal, to finally spatial transformations for data analysis.

4.1 Optics and Setup

For spectroscopy, field of view (FOV) of the detector is integral to the design of a system. Most spectrometers are coupled to the emission using a set of collector lenses and a mirror or a fiber optic cable. Collimators can also be used in front of the fiber optic, but usually reduce light collected. For example, a fiber may have a field of view of 25° and is placed far enough way to see the entire plasma. Thus photons from the entire plasma that enter that FOV cone will be collected by the fiber and thus the sensor. If a collimating or focusing optic is placed in front of the fiber, then only light from the plasma originating from the focal cone of the lens will enter the fiber, which will be less signal than if the fiber saw the entire plasma. This does provide spatial resolution, but reduces signal intensity. Furthermore, if using a fiber optic coupled into a spectrometer, it may not fill up the entire CCD array. In that case, a multi-legged fiber can be used with each pointed at a different spatial location to get temporal and some spatial resolution.

A simple way of testing target location alignment, i.e. if the spectrometer is seeing the location of interest, is to put a pinhole in front of the location of interest. This can be either an actual optic element such as an iris, or simply black cardboard with a hole made by a needle. The pin hole can also be used as a lower cost substitute for a lens array that is focused to a location, assuming the

pinhole can be placed close to the plasma and fully blocks out the rest of the plasma that would be in the spectrometer's FOV. This is likely difficult if the experiment is inside a large vacuum chamber or if the plasma is hot. A common alignment approach is to is to shine a low-power visible laser through the fiber from the spectrometer end. Another approach is using spatially illuminated objects, such as a panel lined with LEDs, in place of the region of interest to determine alignment and FOV. For imaging applications, this approach will allow for detailing focusing of optics and quantifying the FOV and magnification of the measurement.

To get the light out of a vacuum chamber, the two options are either a fiber optic feedthrough, or a window. Glass or quartz windows are common, and readily available for standard 2.75 inch CF flanges. For fiber feedthroughs, the challenge is typically matching the size of the fiber or fiber bundle on either side of the feedthrough to the feedthrough. If there is a mismatch of fiber size, the smallest one will typically limit the light throughput. For example, if the feedthrough has a 100 µm diameter fiber, the in-vacuum fiber has a 600 um diameter fiber, and the in-air fiber has a 200 µm diameter fiber, the feedthrough will attenuate and limit the overall signal. Fiber optics are available in single mode or multimode. Single mode fibers have smaller core diameters, smaller wavelength ranges, and can propagate longer distances. Mulitmode fibers have larger cores, larger wavelength ranges, but have higher signal loss over long distance. For general purpose OES, a multimode fiber is preferable since the fiber lengths in most experimental setups are on the order of meters, which have minimal distance-based signal loss. The second option is typically single or bundled fibers. A fiber bundle has multiple fiber core-cladding sets in a single outer coating. The different cores are usually arranged in either a hexagonal cluster or a line. The bundle is useful because it greatly increases the total amount of light that can be passed. The other end of the bundle can also be bifurcated such that the light can be directed to different sensors, for example two spectrometers that are set for different wavelength ranges.

4.2 Calibrations

A spectroscopy system is composed of multiple components such as detectors, optics, or fibers, that can all attenuate signals and exhibit spectrally selective behaviors. Therefore, calibration of spectroscopy systems and components is requried to ensure validity of measurements as well as transforming the measurements into viable data for applications such as intensity measurements. Calibrations of spectroscopic systems can be separated into three catagories: (1) wavelength, (2) uniformity, and (3) intensity. The calibrations necessary for a spectroscopy system or detector will depend on the application. However, a general best practice is to calibrate for wavelength and intensity frequently as these are generally applicable to most systems and will enable the longevity of collected data for future analysis and applications.

Wavelength calibration is necessary for any spectrally-sensitive detector (such as a spectrometer) as the wavelength is an inferred property as detailed in Section 3. Typically spectrometers come calibrated and with recommendations on how frequestly they need to be recalibrated. However, environmental factors, storage, handling, and other considerations can cause the system to go out of calibration by bumping the grating or sensor, losing motor position, or general position slip over long duration usage. To ensure the measured spectra are accurate to the true wavelengths of emission, a commercially-available calibration lamp (such as a Hg-Ar lamp) with a know spectral output is used as a source and measured with the detector of interest. The measured detector response (i.e. intensity vs time or intensity vs pixel) can then be appropriately adjusted to match the

output spectrum of the calibration lamp to ensure the detector pixel or time conversion to wavelength is accurate. When performing a wavelength calibration, typically only the spectrometer (or other similar detector) needs to be calibrated rather than the system as a whole (the entire optics chain including collection optics) for most applications.

Uniformity calibration is necessary for any spatially-sensitive detector as the response of different regions of the sensor can vary. The purpose of the calibration is to negate out artificial spatial variations in intensity that arise from edge effects of optics, misalignments, and detector noise and sensitivity. The best practice for uniformity calibrations are to use a commercially-available NIST-Traceable Calibration Light Source that has a verified uniform light output. These sources are integrating spheres consisting of a spherical enclosure with different size apertures dictating the size of optics/sensors that can be calibrated. The entire system must be calibrated as a unit since the spatial variations can be affected by components throughout the system, and once calibrated if any components are shifted, swapped, or replaced the entire system must be re-calibrated. For example, a system similar to one shown in Figure 5 would be calibrated by placing the entire system including the inlet optics up to the integrating sphere and ensuring that the entire acquired image is of the inside surface of the source. Images would then be obtained at similar acquisition parameters to those used for true measurements (such as frame size and rates, ISO settings for cameras, temperature and humidity environment of detector) to ensure the applicability of the calibration. The calibration data would provide a mesure of how much intensity varies spatially in the system, and can be subtracted out in the analysis to correct for the artifical system-induced effects.

Intensity calibration is necessary for intensity based measurement techniques and is applicable to all different types of sensors and spectroscopy systems. The calibration has multiple purposes as it can negate out the effects of chromatic sensitivity in systems as well as convert the measurements to quantifiable units for plasma property estimation. The calibration is typically accomplished using a calibrated light source such as the ones used for uniformity calibration in a similar fashion where the entire system as a whole is calibrated. The sources can be operated at tunable luminosity that each have documented intensity as a function of wavelength, enabling spectra measurements to be calibrated from arbitrary counts to standard units such as $\mathrm{W/m^2}$. This is a recommended best practice for measurements of spectra since the measured intensity across wavelengths can differ due to sensitivity of optics, which may introduce inaccuracies and error in applying CRMs to estimate plasma density or temperature.

4.3 Noise Sources and Reduction

Minimizing noise and improving signal is always of interest as it enables reduced uncertainty in measurements and greater temporal or spatial resolution in more complex systems. The most common contributors of noise are dark current and stray light. Dark current refers to the noise generated by the detector's intrinsic and thermal-induced signals in the absence of light. Stray light can occur from various sources in the spectroscopy system, and can usually be resolved by mitigating using encloses around all components and dark surfaces to prevent reflections. However some stray light leaks, including in the plasma environment of interest, may not be preventable. To limit contributions of stray light and/or dark current, the best practice is to collect background scans that can the be subtracted from the measurements. The precise definition of background may vary based on application, but a commonly used approach is to obtain a background scan using identical parameters to the measurement with all conditions of the plasma environment similar aside from

having the discharge on. This will capture all the stray light from the environment affecting the system as well as some representation of dark currents. However, since both these effects can vary between acquisitions, multiple acquisitions are recommended for both the backgrounds and measurements at each setpoint. The scans can the be averaged in post processing to create a measurement that averages out dark current contributions and subtracts out the background stray light contributions.

In some applications, the challenge might be a very weak or low signal instead of high noise levels. In either case, the result is a low signal-to-noise (SNR) that distorts measurements and limits the utility of the data. Weak signals are often encountered in sparse plasma measurements or fast timescale measurements. If the application allows, the easiest way to boost the signal is to use collimating optics to focus the collection. This may narrow the field of view but provide better SNR. Alternatively, larger optics can be used to increase the amount of light collected, or longer exposure for temporally steady plasmas. However, if the application is limited by timescale of the plasma and longer exposures are not tenable, acquisitions of multiple plasma cycles can be summed to resolve the measurement. This in practice can be complicated as it requires the plasma to be repeatable, and a precise triggering system must be used for the measurement, which can be challenging to implement as explained in Section 3.

4.4 Data Transformations

Optical emission spectroscopy measurements are not spatially unique to a point in 3-D space since the optics will collect light from the full volume that exists from the face of the optic thru the full field of view. This 3-D volume is condensed into 2 or 1 dimensions based on the type of method used (imaging vs temporal or spectral), and is typically referred to as ”line-integrated” since the measurement represents the integrated light produced by the entire column of the FOV. If the application does not require depth resolution (such as spectra measurements or measurements in directions free of density gradients), this is not a consideration that significantly affects the intended analysis. However, some techniques, such as imaging or line-ratio estimation, either need depth resolution or may suffer from increased uncertainty in measurements due to unequal line-integrated contributions. In these applications, the line-integration nature can be leveraged to efficiently collect measurements from multiple locations and transformed to yield depth resolution. While this approach introduces setup complexity by requiring motion stages and more extensive data collection, the resulting measurements can produce 2-D or 3-D spatial maps, providing valuable insight at a reduced complexity in comparison to other diagnostic approaches.

The generalized data transformation that enables the geometric reconstruction is the Radon Transform [29]. The transformation takes a function from one plane and projects it onto another plane composed of lines corresponding to line integrals in the original plane. In practice, the function represents an image of interest with the decomposed lines representing chords or lines of sight of the image from different angles. The technique is commononly used in many applications requiring image reconstruction from fixed positions, most notably computed tomography (CT) scanning. In electric propulsion, this technique has been used to reconstruct the plume of a HET in the near-field [30]. Figure 6 shows a summarizing schematic of their approach to reconstruct spatial spectra of the HET plume. In these setups, either a single collection optic or a rake of optics can be positioned to collect chords of light from the plume at an axial location. The collection optics or thruster is then rotated and more measurements taken, with this process repeated to contruct

a contour in theta-space. The collected data would then be calibrated and corrected for any noise considerations. Then, a Radon Transform can be applied (either using user built scripts or functions that exist in MATLAB and Python toolboxes) to transform the data from theta space to Euclidean coordinates and recover the plume image as shown in the figure.

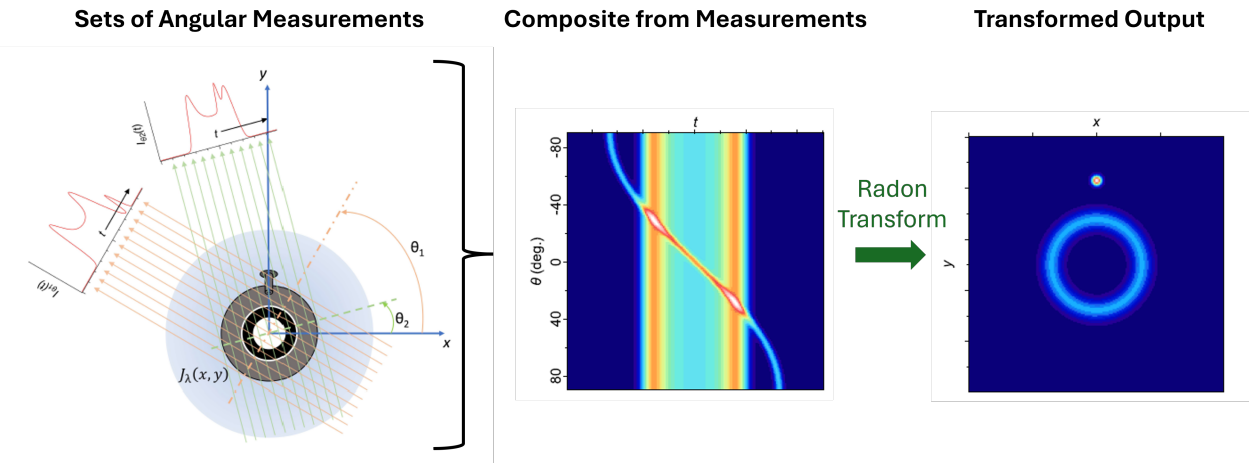

Figure 6: Diagram of CT-style HET plume measurements from Ref. [30] (reproduced with permission). Spectra are collected in line-integrated chords from different azimuthal angles of the plume, with the resulting measurements then Radon transformed to reconstruct a spectral image of the plume.

Experiment designs using the Radon transform do not need to be symmetric due to the mathematical basis, meaning they can be more easily implemented from a geometric standpoint and in cases where the thruster or plume may not be symmetric. However, the need for rotational movement around the thruster or of the thruster can be challenging, especially with larger thrusters or smaller facilities. Additionally, many electric propulsion applications produce axisymmetric plasma environments and that can be leveraged to simplify the experiment setup and analysis. In the case of an axisymmetric function/image/system, the Radon transform simplies to an Abel transform [31]. In these setups, the optic can be swept linearly along an edge of the plasma (or a rake of optics used to collect light) to measure the spatial distribution of line intensity. This shape (or other assumed distributions) can be then applied to back-out the line-resolved intensity distribution of each measurement chord via an Abel inversion (also supported in many programming environments using publically-available toolboxes). If using an Abel inversion, the axisymmetric nature must be kept in mind during the analysis as any experiment setup offsets or individual error measurements will be propagated during the inversion and can result in features in the transformed image.

5 Recommendations

The previous sections have descibed the applications of optical emission spectroscopy traditionally used in electric propulsion, along with the best practices for developing models and laboratory measurements to leverage this powerful technique for insight into plasma processes at play. However, electric propulsion is an ever-developing field and many types of thrusters, fidelity and

capability of models, and better understanding of the plasma processes in play are continually being developed. In this section, specific areas of development in optical emission spectroscopy for electric propulsion are discussed. Recommendations for improvements and advances are detailed to further higher-accuracy of models, and applicability of OES to different types of thrusters and propellants are discussed.

5.1 Collisional-Radiative Model Data Sources

Once the relevant atomic processes have been identified and the energy levels chosen for inclusion in the model, the critical factor determining the accuracy of a CR model's predictions is the accuracy of the collision cross sections and spontaneous transition rates used as inputs. In general, experimental data are preferred over results from quantum mechanical calculations, although in cases for which measurements of only a fraction of the relevant rates are available, some authors have chosen to use a consistent set of theoretical cross sections rather than a mixture of multiple experimental and theoretical sources [14, 16].

The National Institute of Standards and Technology (NIST) Atomic Spectra Database [32] is a valuable resource that compiles experimental data from many publications, providing recommendations for the optimal data sources and reporting quantified uncertainties when available. This database alone is generally sufficient for finding accurate level energies and many of the required spontaneous transition rates (called A_{ki} is the NIST tables), particularly for Xe I. For spontaneous decay rates of Xe II states that have not been measured, the DSBR calculations by Wang et al. [20], which utilized an approach developed over a number of years by Zatsarinny and Bartschat [21, 22], are the best source. Reference [20] is also the only existing source of a sufficiently comprehensive and accurate set of Xe II electron-impact excitation cross sections to enable creation of a Xe II CR model. An extensive set of experimental and theoretical electron-impact excitation cross sections for many elements relevant to general low-temperature plasma research is compiled in the LXCat database [33]; among these are DBSR-calculated cross sections for electron-impact excitation of Xe I [21].

The emission excitation cross sections for Xe I excitations from the ground state to $6p$ states published by Chiu et al. [18] are a high-quality dataset, but prospective users must be aware that cascade contributions are included in these results, and thus excitations to higher states will be double-counted if they are separately included using data from another source. Direct excitation cross sections from the ground state to the Xe I $6p$ levels were previously measured by Fons and Lin [34], and these results were used to calibrate the geometric factor in Chiu's experiment. Jung et al. published experimental cross sections from the Xe I $J = 2$ metastable level to six $6p$ levels [35] and from the ground state and $J = 2$ metastable level to the $7p$ levels [36]. Note that electron-impact de-excitation cross sections may be calculated from the excitation cross sections using the principle of detailed balance [37].

If multiple ionization stages are considered together in a coupled CR model, electron-impact ionization cross sections from the ground state may be needed. Accurate experimental data for single- and multiple-ionization of ground state Xe I were published by Rejoub et al. [38]. Electron-impact ionization can be an important depopulating mechanism for metastable atoms and ions and also for other excited states that have relatively low radiative decay rates. Theoretical cross sections for ionization of metastable Xe I were published by Ton-That and Flannery [39], but recent CR models [14, 16] have chosen instead to use semi-empirical formulas from the Deutsch-Mark

formalism [40], which can be applied to all Xe I and Xe II excited states.

Ion-impact emission excitation cross sections for Xe I (relevant to electric thruster plumes since beam ions have energies well in excess of 100 eV) were measured by Chiu et al. [18] for an ion accelerating voltage of 300 V (producing a Xe^{+} ion beam with 300 eV energy or a Xe^{2+} ion beam with 600 eV energy). The dataset was extended to other ion energies by Sommerville et al. [19]. Ref. [18] also reported cross sections for ion impact ionization-excitation from the Xe I ground state into eight Xe II $6p$ excited states with 300 V ion accelerating voltage and cross sections for electron-impact ionization-excitation over a range of incident electron energies. Since some Xe II $6p$ levels were not included, CR models published to date have had to make assumptions about the values of the missing cross sections based on arguments about similar quantum states [16]. The ionization-excitation cross sections for doubly-charged incident ions automatically include a contribution from asymmetric charge exchange; if the symmetric charge exchange cross section is needed, the best source for xenon is Miller et al. [41].

While most users may choose to develop or use an in-house code to generate a synthetic spectra for OES comparisons, there exist commercial or free programs as well. Below are three example programs; there are others as well and this list is not exhaustive.

1. PrismSPECT is a commercial program with a license fee. It is predominantly a plasma CRM for atomic species with built-in data for hydrogen through argon. Higher Z species may be available by contacting the vendor. It is designed to simulate both LTE and non-LTE plasma.

2. MassiveOE is a free opensource program written in Python to generate and fit plasma emission spectra. It has both atomic and molecular data.

3. NIST LIBS is a database and web-base simulation tool by NIST intended for laser-induced breakdown spectroscopy (LIBS). It can be used to simulate a mixture of multiple elements based on user defined percentages of the mixture. It will provide lines for the first three ionization levels (neutral, singly ionized, doubly ionized) at user defined electron temperature and density.

Going forward, one of the most valuable ways for researchers to advance the state-of-the-art in CR modeling for electric propulsion would be by extending or improving the accuracy of the existing cross section datasets for xenon and other EP-relevant propellants.

5.2 Alternative Propellants

In Section 1, it was prefaced that the majority of this paper focuses on common electric propulsion thrusters and propellants. Historically, xenon has been the most common and ubiquitously used propellant. Therefore modeling and theory development in the community have largely focused on these, with multiple CRMs and datasets of rate coefficients compiled for the propellants. However, recent trends and advancements in EP have diversified the propellants used with these systems. Namely, for Hall thrusters krypton has increasingly become common, specifically in the commercial domain. Additionally, other alternative propellants have become more common such as iodione and indium, along with non-conventional EP systems such as RF ion thrusters, FEEPs, and electrosprays. These propellants do not have substantial theory and modeling available in the literature, and using spectroscopy-based techniques to estimate plasma properties is not currently possible as no CRMs exist. Futhermore, CRMs require cross section datasets that do not currently

exist (or to the variety necessary) for high fidelity models to then enable plasma parameter determination from measurements. Generating cross sections and models for alternative propellants is crucial to the advancement of electric propulsion and OES, and is one of the most useful ways researchers can advance the field.

In the absence of CRMs for alternative propellants, OES can still play a useful role in characterizing discharges and systems utilizing them. Databases and tables, such as the NIST atomic spectra database, do contain numerous identified emission lines for these propellants. These can be utilized along with even simple spectroscopy systems to characterize the relative compositon of plasmas operated on alternative propellants. They can be compared relatively between setpoints or between different propellants on the same system, for example, to qualitatively assess changes in beam divergence or contamination present in the plasma. Using these measurements, potential insight on thruster performance or efficieny can be gleaned and used to assess propellant types and selection for example.

6 Conclusion

In summary, a collaborative set of guidelines, details, and discussion has been presented for optical diagnostic implementation in the laboratory setting for electric propulsion applications. The purpose of this effort was to provide a cohesive and comprehensive overview of how optical emission spectroscopy is utilized in electric propulsion to effectively deduce plasma properties and composition. OES, when used properly, can be a high information-density diagnostic to non-intrusively and passively characterize plasmas. Different types and combinations of spectroscopy systems can be implemeted to provide tailored measurements for each unique application and environment. Additionally, these systems are relatively affordable and simple from a setup and operation perspective, making OES more attractive for wider community adoption across all stages of EP thruster development and characterization. The fundamental and well-understood physcial nature of optical emission in EP plasma environments enables the development of high-fidelity models that can inform the community of plasma processes and dynamics when coupled with experimental measurements. To assist the interplay, measurements must be performed with best practices detailed above in mind to maximize the utility and applicability of the data collected. While the majority of this paper has addressed common electric propulsion systems and associated OES applications, current research and development in the community has created new applications for OES described in Section 5. The fundamental nature of optical emission spectroscopy lends itself well to extension into these new applications such as different propellants and plasma regimes without significant overhaul and redesign of systems to meet diagnostic requirements. Additionally, OES can be a data-rich diagnostic, benefitting greatly from modern advances in computing and data driven models. Leveraging novel techniques and approaches being pursued in other plasma communites in electric propulsion can enable development of multi-line ratio models and improved CRMs to better characterize electric propulsion plasmas and provide greater insight into the fundamental plasma processes driving instabilities and transient behaviors in these systems.

7 Acknowledgments

A portion of this research was carried out at the Jet Propulsion Laboratory, California Institute of Technology, under a contract with the National Aeronautics and Space Administration (80NM0018D0004). The authors would like to thank Professor Kristina Lemmer for her efforts in organizing and managing this series of Recommended Practices in Electric Propulsion papers that this work is a part of.

References

[1] Hutchinson, I. H., "Principles of plasma diagnostics," *Plasma Physics and Controlled Fusion*, Vol. 44, No. 12, 2002, pp. 2603–2603.

[2] Fantz, U., "Basics of plasma spectroscopy," *Plasma sources science and technology*, Vol. 15, No. 4, 2006, p. S137.

[3] Kunze, H.-J., *Introduction to plasma spectroscopy*, Vol. 56, Springer Science & Business Media, 2009.

[4] McWhirter, R., "Spectral intensities," *Plasma diagnostic techniques*, , No. 65, 1965, p. 201.

[5] Griem, H., "Plasma Spectroscopy," *McGraw Hill*, 1964.

[6] Fujimoto, T., "Kinetics of ionization-recombination of a plasma and population density of excited ions. II. Ionizing plasma," *Journal of the physical society of Japan*, Vol. 47, No. 1, 1979, pp. 273–281.

[7] Hagelaar, G., and Pitchford, L. C., "Solving the Boltzmann equation to obtain electron transport coefficients and rate coefficients for fluid models," *Plasma sources science and technology*, Vol. 14, No. 4, 2005, p. 722.

[8] Katz, I., Parks, D., Gardner, B., Mende, S., Collin, H., Manzella, D., and Myers, R., "Spectral line emission by the SEPAC plasma contactor-Comparison between measurement and theory," *33rd Aerospace Sciences Meeting and Exhibit*, 1995, p. 369.

[9] Zhang, Z., Tang, H., Xie, K., and Ouyang, J., "Beam Plasma Expansion of a Helicon Plasma Source," *36th International Electric Propulsion Conference*, Vienna, Austria, 2019.

[10] Karabadzhak, G. F., Chiu, Y.-h., and Dressler, R. A., "Passive optical diagnostic of Xe propelled Hall thrusters. II. Collisional-radiative model," *Journal of applied physics*, Vol. 99, No. 11, 2006.

[11] Celik, M., "Experimental and computational studies of electric thruster plasma radiation emission," Ph.D. thesis, Massachusetts Institute of Technology, 2007.

[12] Dressler, R. A., Chiu, Y.-h., Zatsarinny, O., Bartschat, K., Srivastava, R., and Sharma, L., "Near-infrared collisional radiative model for Xe plasma electrostatic thrusters: the role of metastable atoms," *Journal of Physics D: Applied Physics*, Vol. 42, No. 18, 2009, p. 185203.

[13] Yang, J., Yokota, S., Kaneko, R., and Komurasaki, K., "Diagnosing on plasma plume from xenon Hall thruster with collisional-radiative model," *Physics of Plasmas*, Vol. 17, No. 10, 2010.

[14] Zhu, X.-M., Wang, Y.-F., Wang, Y., Yu, D.-R., Zatsarinny, O., Bartschat, K., Tsankov, T. V., and Czarnetzki, U., "A xenon collisional-radiative model applicable to electric propulsion devices: II. Kinetics of the 6s, 6p, and 5d states of atoms and ions in Hall thrusters," *Plasma Sources Science and Technology*, Vol. 28, No. 10, 2019, p. 105005.

[15] Priti, R., and Srivastava, R., "Collisional-radiative model of xenon plasma with calculated electron-impact fine-structure excitation cross-sections," *Plasma Sources Science and Technology*, Vol. 28, No. 2, 2019, p. 025003.

[16] Chaplin, V. H., Johnson, L. K., Lobbia, R. B., Konopliv, M. F., Simka, T., and Wirz, R. E., "Insights from collisional-radiative models of neutral and singly ionized xenon in Hall thrusters," *Journal of Propulsion and Power*, Vol. 38, No. 5, 2022, pp. 866–879.

[17] Wang, Y.-F., and Zhu, X.-M., "An optical emission spectroscopy method for determining the electron temperature and density in low-temperature xenon plasma by using a collisional-radiative model considering the hyperfine structure of emission line into metastable state," *Spectrochimica Acta Part B: Atomic Spectroscopy*, Vol. 208, 2023, p. 106777.

[18] Chiu, Y.-h., Austin, B. L., Williams, S., Dressler, R. A., and Karabadzhak, G. F., "Passive optical diagnostic of Xe-propelled Hall thrusters. I. Emission cross sections," *Journal of applied physics*, Vol. 99, No. 11, 2006.

[19] Sommerville, J. D., King, L. B., Chiu, Y.-H., and Dressler, R. A., "Ion-collision emission excitation cross sections for xenon electric thruster plasmas," *Journal of Propulsion and Power*, Vol. 24, No. 4, 2008, pp. 880–888.

[20] Wang, Y., Wang, Y.-F., Zhu, X.-M., Zatsarinny, O., and Bartschat, K., "A xenon collisional-radiative model applicable to electric propulsion devices: I. Calculations of electron-impact cross sections for xenon ions by the Dirac B-spline R-matrix method," *Plasma Sources Science and Technology*, Vol. 28, No. 10, 2019, p. 105004.

[21] Zatsarinny, O., and Bartschat, K., "Benchmark calculations for near-threshold electron-impact excitation of krypton and xenon atoms," *Journal of Physics B: Atomic, Molecular and Optical Physics*, Vol. 43, No. 7, 2010, p. 074031.

[22] Zatsarinny, O., and Bartschat, K., "The B-spline R-matrix method for atomic processes: application to atomic structure, electron collisions and photoionization," *Journal of Physics B: Atomic, Molecular and Optical Physics*, Vol. 46, No. 11, 2013, p. 112001.

[23] Bogaerts, A., Gijbels, R., and Vlcek, J., "Collisional-radiative model for an argon glow discharge," *Journal of applied physics*, Vol. 84, No. 1, 1998, pp. 121–136.

[24] Xu, G., "Diagnostics of Plasmas and Gases," *2019 AIAA SciTech Forum*, 2019.

[25] Nakles, M. R., Holmes, M. R., and Hargus Jr, W. A., "An investigation into the spectral imaging of Hall thruster plumes," Tech. rep., 2015.

[26] Konopliv, M. F., Johnson, L. K., and Wirz, R. E., "Ion-neutral phasing in Hall thruster breathing mode oscillations," *Journal of Applied Physics*, Vol. 136, No. 22, 2024.

[27] Konopliv, M. F., Johnson, L. K., and Wirz, R. E., "Time-resolved electron temperature oscillations in Hall thrusters," *Journal of Applied Physics*, Vol. 137, No. 24, 2025.

[28] Osin, D., and Schindler, T., "Dual wavelength imaging of a scrape-off layer in an advanced beam-driven field-reversed configuration," *Review of Scientific Instruments*, Vol. 87, No. 11, 2016.

[29] Toft, P. A., "The Radon transform-theory and implementation," 1996.

[30] Nakles, M. R., and Matlock, T. S., "Hall thruster near-field plume characterization through optical emission spectroscopy," *36th Int. Electric Propulsion Conf.*, 2019, pp. p–IEPC.

[31] Vest, C., "Formation of images from projections: Radon and Abel transforms," *Journal of the Optical Society of America*, Vol. 64, No. 9, 1974, pp. 1215–1218.

[32] Kramida, A., Ralchenko, Y., Reader, J., and Team, N. A., "NIST Atomic Spectra Database (ver. 5.12)," , 2024. URL `http://physics.nist.gov/asd`.

[33] Carbone, E., Graef, W., Hagelaar, G., Boer, D., Hopkins, M. M., Stephens, J. C., Yee, B. T., Pancheshnyi, S., Van Dijk, J., and Pitchford, L., "Data needs for modeling low-temperature non-equilibrium plasmas: the LXCat project, history, perspectives and a tutorial," *Atoms*, Vol. 9, No. 1, 2021, p. 16.

[34] Fons, J. T., and Lin, C. C., "Measurement of the cross sections for electron-impact excitation into the 5 p 5 6 p levels of xenon," *Physical Review A*, Vol. 58, No. 6, 1998, p. 4603.

[35] Jung, R., Boffard, J. B., Anderson, L., and Lin, C. C., "Electron-impact excitation cross sections from the xenon J= 2 metastable level," *Physical Review A—Atomic, Molecular, and Optical Physics*, Vol. 72, No. 2, 2005, p. 022723.

[36] Jung, R., Boffard, J. B., Anderson, L., and Lin, C. C., "Excitation into 5 p 5 7 p levels from the ground level and the j= 2 metastable level of xe," *Physical Review A—Atomic, Molecular, and Optical Physics*, Vol. 80, No. 6, 2009, p. 062708.

[37] Rybicki, G. B., and Lightman, A. P., *Radiative processes in astrophysics*, John Wiley & Sons, 2024.

[38] Rejoub, R., Lindsay, B., and Stebbings, R., "Determination of the absolute partial and total cross sections for electron-impact ionization of the rare gases," *Physical Review A*, Vol. 65, No. 4, 2002, p. 042713.

[39] Ton-That, D., Flannery, M., and Manson, S., "Cross sections for excitation and ionization in e-He (21, 3S) collisions," *Journal of Physics B: Atomic and Molecular Physics*, Vol. 10, No. 4, 1977, p. 621.

[40] Deutsch, H., Scheier, P., Becker, K., and Märk, T., "Revised high energy behavior of the Deutsch-Märk (DM) formula for the calculation of electron impact ionization cross sections of atoms," *International Journal of Mass Spectrometry*, Vol. 233, No. 1-3, 2004, pp. 13–17.

[41] Miller, J. S., Pullins, S. H., Levandier, D. J., Chiu, Y.-h., and Dressler, R. A., "Xenon charge exchange cross sections for electrostatic thruster models," *Journal of Applied Physics*, Vol. 91, No. 3, 2002, pp. 984–991.